

The Visualization Simulation Platform Development for OFDM-Based Visible Light Communication in Indoor Application

Chuang Kwang Seng¹, Rahmat Talib^{1*}

¹Department of Electronic Engineering, Faculty of Electrical and Electronic Engineering,
Universiti Tun Hussein Onn Malaysia, Batu Pahat, 86400, MALAYSIA

*Corresponding Author Designation

DOI: <https://doi.org/10.30880/eeee.2021.02.02.050>

Received 04 July 2021; Accepted 09 August 2021; Available online 30 October 2021

Abstract: In the VLC system study, simulation and prototype development are the important processes to build up an OFDM-based visible light communication system for indoor application. However, prototype development is time-consuming and costly. This paper proposed a MATLAB graphical user interface (GUI) for orthogonal frequency division multiplexing (OFDM) based visible light communication in a room dimension of 6m*6m*3.5m. For the proposed GUI, visible light modelling was employed to obtain received power from line-of sight and first reflection from wall by considering average power transmitted per LED was 115mW. Then total received power is used to investigate the signal-to-noise ratio (SNR) and calculate the bit error rate (BER) based on the 4-QAM modulation technique. In addition, the delay spread profile is examined. The simulation results showed that transmitters' position along the x-axis given the lowest delay spread profile compared to axis-excited topology and corner-excited topology. In the future, the application of indoor positioning could be added to increase the functionalities of GUI. Further performance analysis possible to be included are the SNR, BER and indoor positioning accuracy.

Keywords: Visualization Simulation Platform, OFDM, Signal-to-Noise Ratio, Bit Error Rate

1. Introduction

Visible light communication is the oldest kind of communication in the past by using fire and Sun reflection. But the development in communication sciences and the increasing demand for mobile communications have made the radio frequency band very crowded. In addition, radio frequency-based communications suffered multipath propagation, which reduced the link availability and performance. Light-emitting diodes (LEDs) lamps in switching and modulating light signals from an electrical signal at high speed utilized visible light, becoming a potential solution for wireless communication.

VLC offered several attractive advantages: energy conservation, cost-effectiveness, excellent security, high bandwidth capacity, and the absence of electromagnetic interference [1]. Indoor VLC commonly uses LEDs as transmitters and photodiodes as receivers. In an indoor environment, numerous LEDs overlap, resulting in inter-symbol interference (ISI). OFDM is efficient in terms of bandwidth usage because it split the bandwidth into orthogonal, which overlapped subcarrier has been applied in VLC. With introducing a cyclic prefix (CP), OFDM has the intensity to combat ISI [2].

The signal to noise ratio (SNR) at the receiver by configuring the transmitter's semi-angle at half power, the field of view (FOV) at the detector, transmitter's array size and location are explored in [3]. The power delay profile (PDP) at different transmitter topologies was evaluated and the RMS delay spread profile was plotted in [4]. The effect of multipath reflection on the channel characterization and bit error rate (BER) analysis was emulated in [5]. There are a lot of parameters that affect the performance of the OFDM-based VLC system. The power distribution, RMS delay spread, SNR and BER are crucial analysis for the system. Hence, a visualization simulation platform is needed to help the students or practiced professionals to investigate the performance of OFDM-based visible light communication in a more comprehensive way which the effect of each parameter can be analyzed intensively and possible to upgrade the mathematical model directly.

2. Materials and Methods

The proposed Graphical User Interface (GUI) was developed by using MATLAB R2020b App Designer. The algorithm for received optical power with first reflection and RMS delay spread is stated in [4], the formula for signal to noise ratio is stated in [6] and the expression of bit error rate based on the 4-QAM technique is stated in [7] are adopted to develop the GUI. The GUI was verified by obtaining the result simulated with the same parameter in previous studies.

2.1 Software design

Figure 1 shows the flow chart of MATLAB GUI. The received power on the LOS channel and first reflection channel based on the input parameter value was first calculated. The received power distribution calculated was then applied in SNR and BER calculation. Lastly, the RMS delay spread was also calculated.

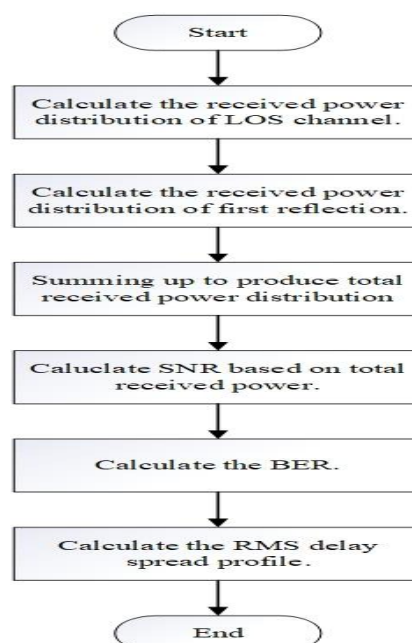


Figure 1: Flow chart of the GUI

2.2 GUI design

The parameter configuration tab as shown in Figure 2. From the tab, the user is allowed to key in the transmitters’ position by referring to the x-axis (-3 to 3) and y-axis (-3 to 3). User also allow to configure the field of view at the detector, the detector physical area, the semi-angle at half power of LED, the reflection coefficient of the wall and the bit rate of the transmitted signal. The ‘Execute’ push-button is pressed to calculate and plot the result at each tab accordingly. The ‘Reset’ push-button clear all the inserted value and the plotted result.

The power distribution tab as shown in Figure 3 is designed to calculate the received power on the receiver plane based on line-of-sight (LOS) and fist reflection from the walls. The maximum and minimum received power are also displayed in dBm. The equations to calculate the received power are listed in Eq.1 [8].

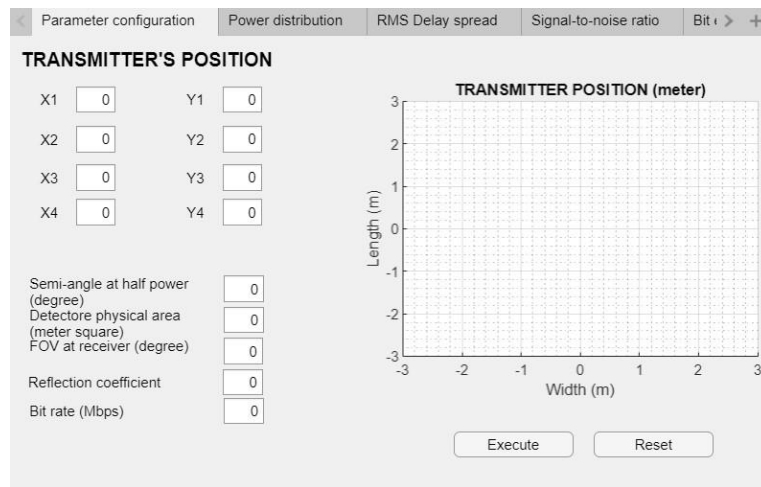


Figure 2: Parameter configuration tab



Figure 3: Power distribution tab

The power distribution

$$P_r = \sum^{N_{LEDs}} \left\{ P_t H_d(0) + \int_{Reflections} P_t dH_{ref}(0) \right\} \tag{Eq. 1}$$

where P_r is total received power, P_t is the total transmitted power, $H_d(0)$ represent channel gain of LOS and $H_{ref}(0)$ is the channel gain of first reflection from the walls.

The channel gain of LOS is listed in Eq.2[9].

$$H_d(0) = \begin{cases} \frac{A(m+1)}{2\pi d^2} \cos^m(\Phi) T_s(\Psi) g(\Psi) \cos(\Psi), & 0 \leq \Psi \leq \Psi_c \\ 0 & \text{elsewhere } \Psi > \Psi_c \end{cases} \quad \text{Eq. 2}$$

where Φ is the angle of irradiance at the transmitter, A is the physical area of the photodiode detector (PD), $g(\Psi)$ is the optical concentrator gain, d is the distance between the transmitter and the receiver, Ψ_c denotes the range of the field of view at receiver, $T_s(\Psi)$ is the gain of the optical filter.

The first reflection’s channel gain is listed in Eq.3.

$$H_{ref}(0) = \begin{cases} \frac{A(m+1)}{2(\pi d_1 d_2)^2} \rho d A_{wall} \cos^m(\Phi_r) \cos(\alpha_{ir}) \times \\ \cos(\beta_{ir}) T_s(\Psi) g(\Psi) \cos(\Psi_r), & 0 \leq \Psi_r \leq \Psi_c \\ 0, & \text{elsewhere } \Psi_r > \Psi_c \end{cases} \quad \text{Eq. 3}$$

where d_1 is the distance between a lamp and a reflective point, d_2 is the distance between a reflective point and a receiver surface, dA_{wall} is a reflective area of a small region, ρ is the reflectance factor, β_{ir} are the angle of irradiance to the receiver and Φ_r is the angle of irradiance to a reflective point, respectively and Ψ_r is the angle of incidence from the reflective surface.

The expression for Lambertian emission represented by m is listed in Eq.4.

$$m = \frac{\ln(2)}{\ln(\cos \Phi_{1/2})} \quad \text{Eq. 4}$$

where $\Phi_{1/2}$ is the semi-angle at half power of LED.

The expression for the optical concentrator’s gain at detector is listed in Eq.5.

$$g(\Psi) = \begin{cases} \frac{n^2}{\sin^2 \Psi_c}, & 0 \leq \Psi \leq \Psi_c \\ 0, & 0 \geq \Psi_c \end{cases} \quad \text{Eq. 5}$$

where n is known as refractive index.

The RMS delay spread tab as shown in Figure 4 is designed to calculate and plot the delay spread profile. The maximum RMS delay spread is displayed in nanoseconds (ns) and the maximum permissible bit rate state in Mbps. The RMS delay is a key efficiency requirement for the data transmission’s upper limit. The mean excess delay is listed in Eq.6 [4].

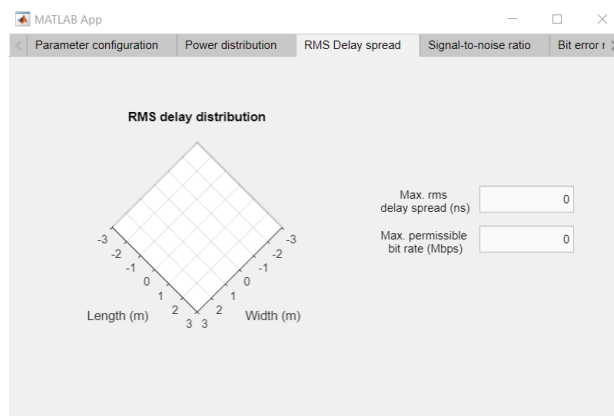


Figure 4: RMS delay spread tab

The mean excess delay

$$\mu = \frac{\sum_{i=1}^M P_{d,i} t_{d,i} + \sum_{j=1}^N P_{ref,i} t_{ref,j}}{P_{rT}} \tag{Eq. 6}$$

$$\mu^2 = \frac{\sum_{i=1}^M P_{d,i} t_{d,i}^2 + \sum_{j=1}^N P_{ref,i} t_{ref,j}^2}{P_{rT}} \tag{Eq. 7}$$

where P_{rT} is the total received power for both LOS and first reflection from the walls, $P_{ref,j}$ is the received power from the j^{th} reflected line and $P_{d,i}$ is received power from the i^{th} direct line.

The RMS delay profile is listed in Eq.8

$$D_{RMS} = \sqrt{\mu^2 - (\mu)^2} \tag{Eq. 8}$$

The signal-to-noise ratio tab as shown in Figure 5 is designed to calculate and plot signal-to-noise ratio (SNR) based on the received power obtained. The maximum and minimum signal-to-noise ratio on the receiver plane is stated in dB. The SNR can express in terms of liability of detector, received power and noise variance, by assuming the noise from solar radiation and other illuminance sources. The expression is listed in Eq.9 [10].

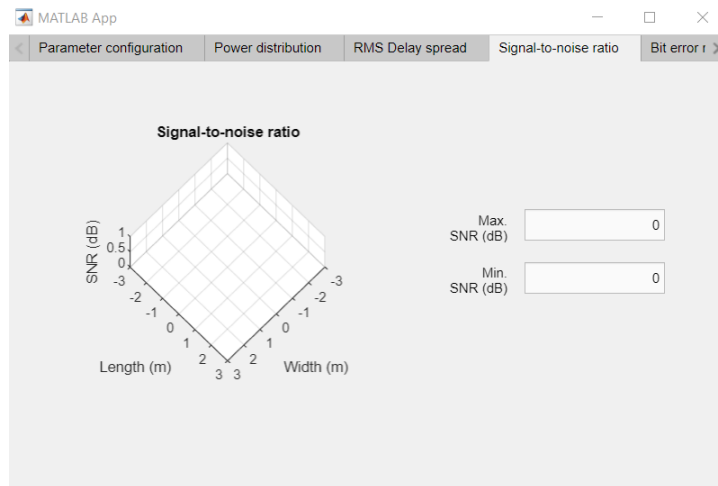


Figure 5: Signal-to-noise ratio tab

The SNR expression

$$SNR = \frac{(RP_r)^2}{\sigma_{shot}^2 + \sigma_{thermal}^2} \tag{Eq. 9}$$

The shot and thermal noise variances is listed in Eq.10 and Eq.11.

$$\sigma_{thermal}^2 = \frac{8\pi\kappa T_K}{G_{ol}} C_{pd} A I_2 B^2 + \frac{16\pi^2\kappa T_K \Gamma}{g_m} C_{pd}^2 A^2 I_3 B^3 \tag{Eq. 10}$$

$$\sigma_{shot}^2 = 2qBR(P_r + P_{r-isi}) + 2qBI_2 I_3 \tag{Eq. 11}$$

where B is the noise bandwidth in Hz, q is the charge of the electron in coulomb, T_k is absolute temperature, κ is the Boltzmann's constant, I_B is the photocurrent cause by background radiation, G_{ol} is the open-loop voltage gain, Γ is the FET channel noise factor, C_{pd} is the fixed capacitance of detector per unit area, g_m are the FET transconductance and noise bandwidth factors I_2 and I_3 .

The bit error rate tab as shown in Figure 6 is designed to calculate and plot the bit error rate (BER) based on 4-QAM technique. The maximum and minimum value of bit error rate are stated. The expression of BER performance based on M-QAM is listed in Eq.12 [7].

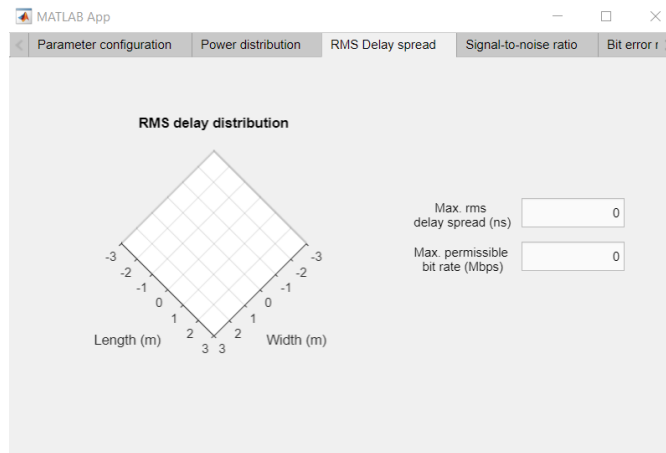


Figure 6: Bit error rate tab

The BER expression

$$BER = \frac{4(\sqrt{m}-1)}{\sqrt{M} \log_2 M} Q \left(\sqrt{\frac{3}{M-1}} SNR \right) \tag{Eq. 12}$$

where Q is the Gaussian Q-function. Eq.13 is listed below.

$$Q(x) = \frac{1}{\sqrt{2\pi}} \int_x^\infty e^{-\frac{y^2}{2}} dy \tag{Eq. 13}$$

2.3 Lamp layout

The 4 lamps were installed at height of 3.5m and placed at (-1.5, -1.5), (-1.5, 1.5), (1.5, -1.5) and (1.5, 1.5) as showed in Figure 7 known as corner-excited topology.

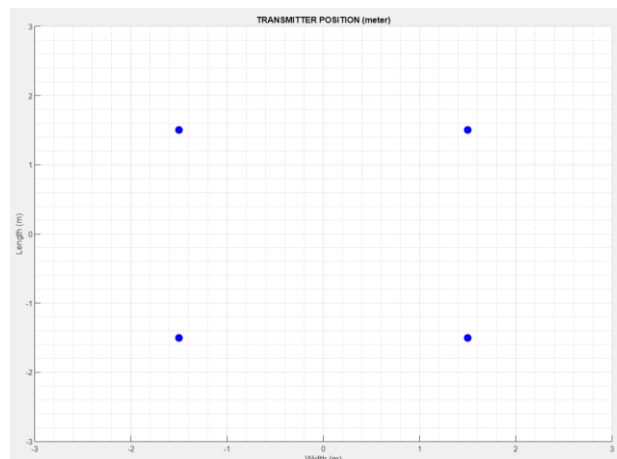


Figure 7: Corner excited topology

The 4 lamps were installed at height of 3.5m and placed at (-1.5, 0), (0, 1.5), (0, -1.5) and (1.5, 0) as showed in Figure 8 known as axis-excited topology.

The 4 lamps were installed at height of 3.5m and placed at (-1.5, 0), (-0.5, 0), (0.5, 0) and (1.5, 0) as showed in Figure 9 known as lamps' position along x-axis.

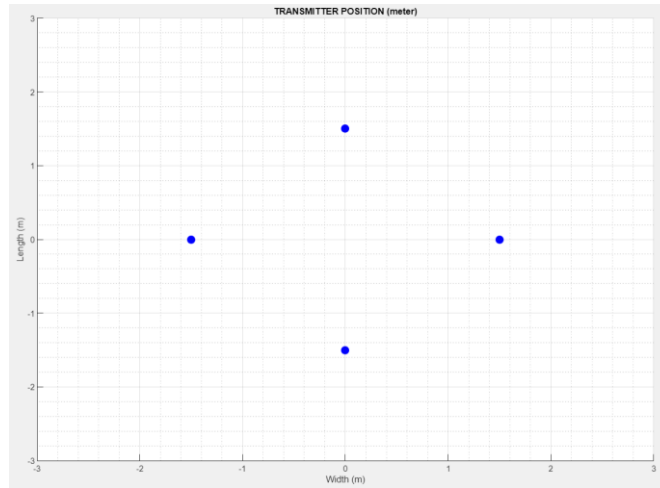


Figure 8: Axis-excited topology

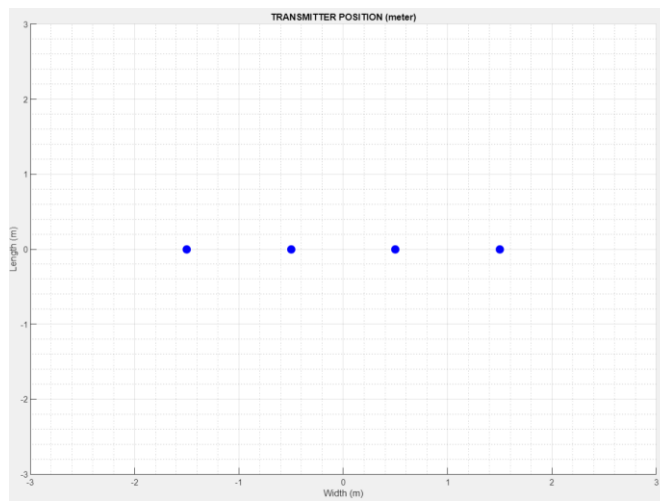


Figure 9: Lamps' position along x-axis

3. Results and Discussion

The corner-excited topology has the maximum received power with the first reflection was 0.3926 dBm and the minimum was -4.219 dBm. The 3D plot for received power in Figure 10. Figure 11 shows the delay spread profile of the topology with a maximum of 2.718 ns and an average of 1.83

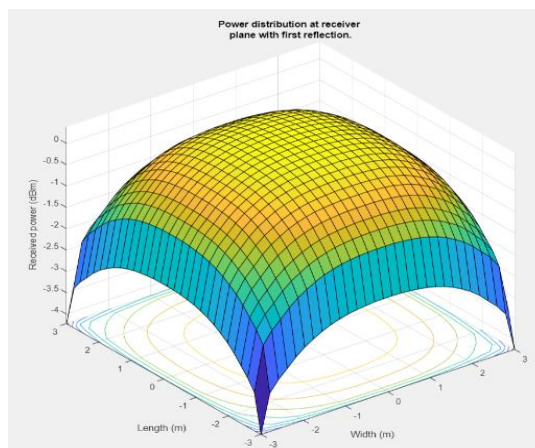


Figure 10: Received power of corner-excited topology

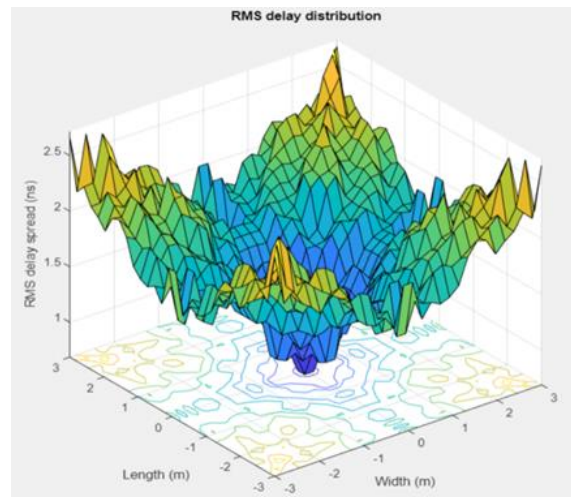


Figure 11: RMS delay spread of corner-excited topology

The maximum received power with the first reflection for corner-excited topology was 1.31 dBm and the minimum was -4.763 dBm. The 3D plot for received power in Figure 12. Figure 13 shows the view of RMS delay spread for axis-excited topology with a maximum of 2.131 ns and an average of 1.558 ns.

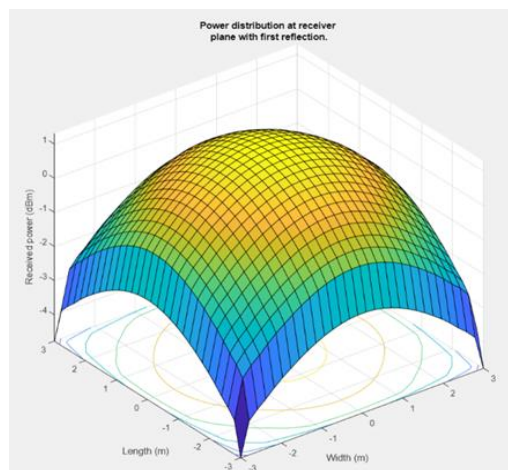


Figure 12: Received power of axis-excited topology

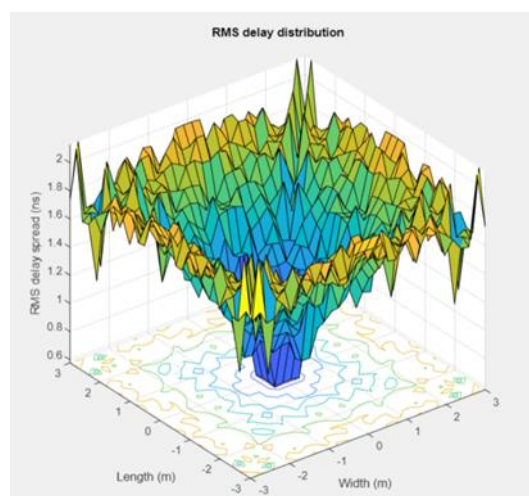


Figure 13: RMS delay spread of axis-excited topology

The lamps' position along the x-axis has the maximum received power with the first reflection was 1.814 dBm and the minimum was -4.904 dBm. The 3D plot for received power in Figure 14. Figure 15 shows the view of RMS delay spread for axis-excited topology with a maximum of 1.739 ns and an average of 1.157 ns.

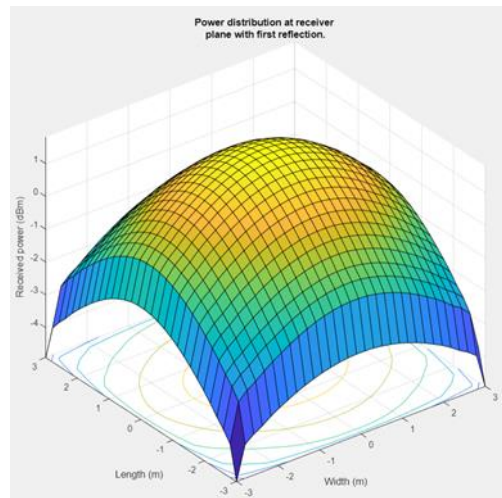


Figure 14: Received power of lamps' position along x-axis

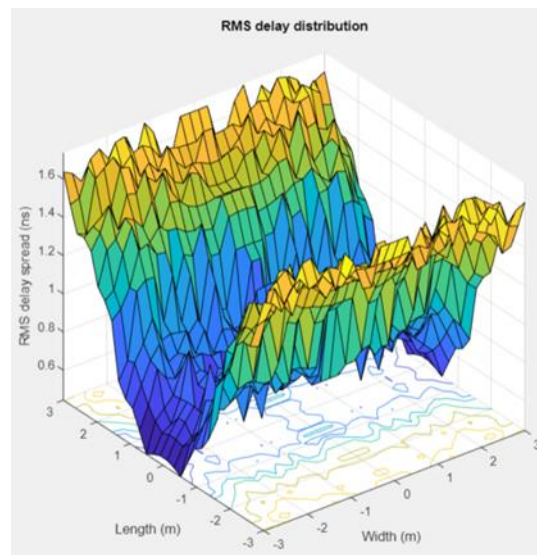


Figure 15: RMS delay spread of lamps' position along x-axis

Table 1 shows the received power and RMS delay on 3 topologies. From Figures 10, 12 and 14, the lamps' position along the x-axis has the lowest RMS delay spread for both maximum and average, and the corner-excited topology has the most significant RMS delay spread for both maximum and average. Lamps' position along x-axis topology is most suitable topology for VLC in the room because it can achieve the highest maximum permissible data rate according to the lowest maximum RMS delay spread. However, the corner-excited topology have the lowest standard deviation for received power with first reflection, which means the power distribution is the most uniform. In the lamps' position along the x-axis, the RMS delay spread experienced its minimum along the x-axis. This result due to the lesser symmetry between the lamps and reflective wall. The symmetry between lamps and reflective walls resulted in constructive interference, which maximizing the RMS delay spread. The minimum RMS delay spread occurred at the center of the room for both corner-excited and axis-excited topology

because of the faded away of reflective optical ray due to the extended distance from the reflective walls.

Table 1: Received power and RMS delay on 3 topologies

Lamps' topology	Received power with first reflection (dBm)			RMS delay spread (ns)	
	Maximum	Minimum	Standard deviation	Maximum	Mean
Corner-excited	0.393	-4.219	0.013	2.718	1.830
Lamps' position along x-axis	1.814	-4.904	0.022	1.739	1.157
Axis-excited	1.310	-4.763	0.063	2.131	1.558

4. Conclusion

In conclusion, an OFDM-based visible light communication algorithm was developed by assuming average transmitted power per LED after OFDM was 115mW and 4-QAM techniques. A graphical user interface (GUI) for visible light communication system analysis with room dimension of 6m*6m*3.5m and receiver plane on floor level designed with MATLAB App Designer. The GUI allowed users to configure semi-angle at half power of transmitters, the field of view at the detector, physical detector area, the reflection coefficient of the wall, and the bit rate. Performance analysis of OFDM-based visible light communication in the room carried out with various lamps' topology. The received power with first reflection and RMS delay spread were evaluated. The simulation results obtained the lamps' position along the x-axis gave the lowest RMS delay spread compared to corner-excited topology and axis-excited topology. It can conclude that the lamps' position along the x-axis is most suitable for VLC in the room because of the highest maximum permissible data rate. However, the coverage of the power distribution should be a concern.

Acknowledgement

The authors would like to thank the Faculty of Electrical and Electronic Engineering, Universiti Tun Hussein Onn Malaysia for its support.

References

- [1] L. E. M. Matheus, A. B. Vieira, L. F. M. Vieira, M. A. M. Vieira, and O. Gnawali, "Visible Light Communication: Concepts, Applications and Challenges," *IEEE Commun. Surv. Tutorials*, vol. 21, no. 4, pp. 3204–3237, 2019.
- [2] M. Alhalabi, F. I. El-Nahal, and N. Taspinar, "Comparison of different modulation techniques for optical OFDM Intensity Modulation and Direct Detection IM/DD system," in *2019 IEEE 7th Palestinian International Conference on Electrical and Computer Engineering (PICECE)*, 2019, pp. 1–4.
- [3] F. Madani, G. Baghersalimi, and Z. Ghassemlooy, "Effect of transmitter and receiver parameters on the output signal to noise ratio in visible light communications," *2017 25th Iran. Conf. Electr. Eng. ICEE 2017*, pp. 2111–2116, 2017.
- [4] S. S. Muhammad, "Delay profiles for indoor diffused visible light communication," *Proc. 13th Int. Conf. Telecommun. ConTEL 2015*, no. 2, pp. 1–5, 2015.

- [5] R. Raj, S. Jaiswal, and A. Dixit, "On the Effect of Multipath Reflections in Indoor Visible Light Communication Links: Channel Characterization and BER Analysis," *IEEE Access*, vol. 8, pp. 190620–190636, 2020.
- [6] P. H. Pathak, X. Feng, P. Hu, and P. Mohapatra, "Visible Light Communication, Networking, and Sensing: A Survey, Potential and Challenges," *IEEE Commun. Surv. Tutorials*, vol. 17, no. 4, pp. 2047–2077, 2015.
- [7] I. Stefan, H. Elgala, and H. Haas, "Study of dimming and LED nonlinearity for ACO-OFDM based VLC systems," *IEEE Wirel. Commun. Netw. Conf. WCNC*, pp. 990–994, 2012.
- [8] T. Komine and M. Nakagawa, "Fundamental analysis for visible-light communication system using LED lights," *IEEE Trans. Consum. Electron.*, vol. 50, no. 1, pp. 100–107, 2004.
- [9] C. Ley-Bosch, I. Alonso-Gonzalez, D. Sanchez-Rodriguez, and M. A. Quintana-Suarez, "Analysis of the effects of the hidden node problem in IEEE 802.15.7 uplink performance," *IEEE CITS 2015 - 2015 Int. Conf. Comput. Inf. Telecommun. Syst.*, pp. 1–5, 2015.
- [10] N. A. Tran, V. V. Mai, T. C. Thang, and A. T. Pham, "Impact of reflections and ISI on the throughput of TCP over VLC networks with ARQ-SR protocol," *4th Int. Conf. Photonics, ICP 2013 - Conf. Proceeding*, no. 1, pp. 172–174, 2013.